

Synthesis and Characterisation of Non-Stoichiometric Hydroxyapatite Nanoparticles for Potential Bone Replacement and Regeneration Applications

Aqif Anwar Chaudhry,^{a,*} Nida Iqbal Khan,^a Rabia Nazir,^a Rafaqat Hussain,^a Abdul Samad Khan,^{a,b} Ihtesham-ur-Rehman,^{a,c} Ali Abdullah,^d M. Anis-ur-Rehman^d

^a Interdisciplinary Research Centre in Biomedical Materials, COMSATS Institute of Information Technology, Defence Road, Off Raiwind Road, Lahore

^b Department of Materials, Queen Mary University of London, Mile End Road, London, UK – E1 4NS

^c The Kroto Research Institute, North Campus, University of Sheffield, Broad Lane, Sheffield S3 7HQ

^d Applied Thermal Physics Laboratory, Department of Physics, COMSATS Institute of Information Technology, Chak Shahzad Campus, Islamabad

*Corresponding author e-mail: aqifanwar@ciitlahore.edu.pk

Hydroxyapatite is similar to biological apatite, the mineral component of bone. Efforts in the seventies and eighties popularised its commercial use as an ideal bone substitute. It was part of the approach-shift from bioinert materials to bioactive materials for bone replacement and regeneration. However, more than three decades later, research on calcium phosphates is almost non-existent and their applications in surgery are very rare due to extremely high import prices unaffordable by the masses of Pakistan. This paper outlines the synthesis of non-stoichiometric hydroxyapatite and its detailed characterisation using Scanning Electron Microscopy, X-ray Diffraction, Raman and Fourier Transform Infra Red Spectroscopy. These revealed the synthesised apatitic phase to be non-stoichiometric hydroxyapatite containing substituted carbonate ions in its as-precipitated form. Overall, this paper outlines one the first detailed attempts at knowledge creation regarding hydroxyapatite in Pakistan and should be instrumental in introduction of this material for subsequent surgical use in the country.

Introduction

Hydroxyapatite [HA, Ca₁₀(PO₄)₆(OH)₂] is a synthetic calcium phosphate ceramic chemically similar to biological apatite the mineral component of bone.¹ Due to this similarity, it has been widely used as a bone substitute. Although the first instance of use of a calcium phosphate for bone repair dates back to 1920 serious efforts were taken half a century later to commercialize the use of hydroxyapatite (during the seventies and eighties).² The leading research groups at that time were headed by Larry. L. Hench and Hideki Aoki, respectively.^{3,4} The fundamental principle behind usage of HA in bone replacement and regeneration applications is its excellent biocompatibility and bioactivity.

In late sixties and seventies Hench demonstrated through his research that a biomaterial should be preferably bioactive as opposed to the traditional approach wherein bioinert materials were used.^{3,5} Most bioglasses and calcium phosphate all behave in a bioactive manner wherein a positive interaction takes place between the implant surface and the surrounding tissue.⁶ Calcium phosphates rely on the localized calcium and phosphorus ion super saturations as a result of their surface dissolution (this enhances bone cell activity) in the defect environment where bone forming cells perform their typical repair functions.⁶ More so, it is also possible to tailor the composition of these calcium phosphates to increase the activity of bone forming cells in order to form the aforementioned bond quicker; hence resulting in quicker healing and reduced patient bed rest times. HA therefore, has been used as a bone filler, reinforcement in polymer matrices and also in the form of coatings.^{4,7} For the aforementioned

applications various HA morphologies have been used ranging from nanoparticles, sintered granules (and their pastes in appropriate liquids) to porous scaffolds. HA can be synthesised using a large variety of techniques each having their advantages and short falls. Wet-chemical methods include co-precipitation, batch and continuous hydrothermal synthesis, sol-gel method and emulsion techniques.⁸⁻¹² HA has also been synthesised using solid state methods and CVD technology.^{13,14} The key to synthesis of hydroxyapatite is control over reaction parameters which ascertain the degree of stoichiometry in the resulting phase. Stoichiometry in HA has a direct link to its thermal stability, in-vitro and in-vivo dissolution and mechanical strength. Failure to carefully monitor reaction parameters often results in formation of other calcium phosphate phases upon heating. However, depending on the application, these thermal by-products may offer desirable properties such as enhanced dissolution in the case of beta-tricalcium phosphate.¹⁵ Given the absence of any formal calcium phosphate line of treatment in Pakistan there is a dire need to develop non-stoichiometric calcium phosphates for enhanced dissolution and quicker bone repair in the body that may result in reduced patient bed rest times.

This work presents the synthesis and characterisation of non-stoichiometric HA and attempts to achieve porosity in its sintered form. In all these varying morphologies, HA offers wide ranging properties, making it suitable for bone filling, coatings on metallic substrates and as scaffolds for guide bone regeneration.

Materials and Methods

Calcium nitrate tetrahydrate [99.0%] was obtained from Unichem India. Diammonium hydrogen phosphate [96-102%] was

obtained from AppliChem Germany. Ammonium hydroxide (35% BDH) was used to adjust the pH of the solutions prior to reaction and also during and after addition and mixing of reagents. Concentration of calcium nitrate and diammonium hydrogen phosphate solutions were such that the Ca:P molar ratio was 1.67 [according to the formula $\text{Ca}_{10}(\text{PO}_4)_6(\text{OH})_2$].

Dropwise mixing of 0.2 M CaN and 0.12 M DAHP solutions made in deionized water (whilst maintaining pH 10) resulted in formation of a suspension that was aged overnight (21 hours). The suspension was then filtered, washed and oven dried to result in a free flowing powder labelled as HA. This powder was then

per step. Crystallite size of a corresponding phase was calculated using the Scherrer Equation:

$$d = (0.94 \lambda) / (B \cos\theta)$$

where d is the crystallite size, B is the full width at half maximum (using the most intense peak of the corresponding phase) and λ is the wavelength of the Cu- α radiation (1.542 Angstroms).

Raman spectra were collected using a Nicolet Almega Dispersive Raman Spectrometer averaging 128 scans and 10 seconds scan time. Fourier Transform Infra Red (FTIR) data was collected using a photoacoustic cell in a Nicolet FTIR 800 spectrometer

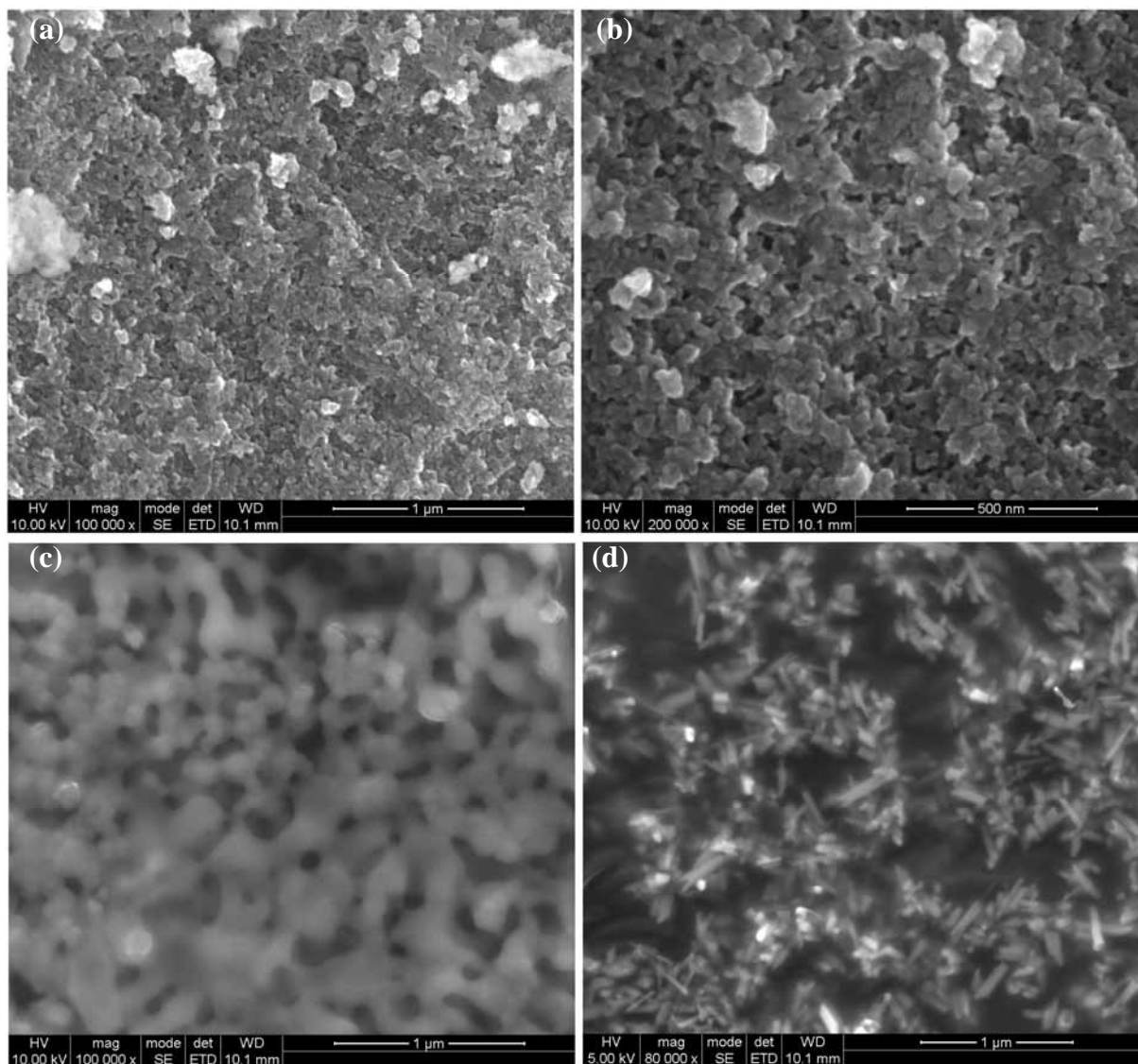


Figure 1 Scanning Electron Microscope images of as precipitated sample A at (a) x100K magnification [bar = 1 micron] (b) at x200K magnification [bar = 500 nm] (c) sample A heat-treated at 900 °C for 1 hour (c) at x100K magnification [bar = 1 micron] and HA nanorods [synthesis reported elsewhere by the authors] at (d) x80K magnification [bar = 1 micron]

heat treated at 900 °C for 1 hour and is hereby labelled as HA900.

Scanning Electron Microscope (SEM) images were collected using a FEI Inspect F SEM. Powder X-ray Diffraction (PXRD) patterns for all samples were observed using a X-Pert Pro PW 3050/60 diffractometer using a 0.02° step size and 0.15 seconds

averaging 128 scans with 8 cm^{-1} spectral resolution.

Results and Discussion

Figures 1 (a)-(c) shows the SEM images of samples HA and HA900. In Figure 1 (a) and 1 (b) it was observed that HA

comprised of nanosized particles [avg. 35 nm ± 10 nm, 50 particles sampled]. The nanoparticles were agglomerated and had a rounded morphology. Heat-treatment of HA at 900 °C for 1 hour led to sintering of these nanoparticles into hard porous agglomerates [larger than 5 μm in size as observed in Figure 1(c)]. On observation it can be seen that this agglomerated fused form comprises of smaller nanoparticles linked to each other to form a larger network. This linkage, known as necking, is part of the sintering process. The morphology of the as-precipitated nanoparticles is different from the traditionally seen needle-like shape in literature. The authors reported rod-like nanoparticles for stoichiometric HA made using continuous hydrothermal synthesis in a previous communication [as seen in Figure 1(d)].⁹ This difference in morphology can be attributed to the possible non-stoichiometry of the resulting apatitic phase and also the nature of the processes wherein the current work is a batch process with low diffusivity (hence more agglomeration) and CHFS is a flow process with high diffusivity (hence less agglomeration). Such a degree of agglomeration [as seen in Figure 1(a) and (b)] is desirable as heat-treatment leads to formation of porous hard agglomerates. Further heat-treatment should facilitate formation of granules which are the preferred form of powders used as bone fillers in surgery today.¹⁶

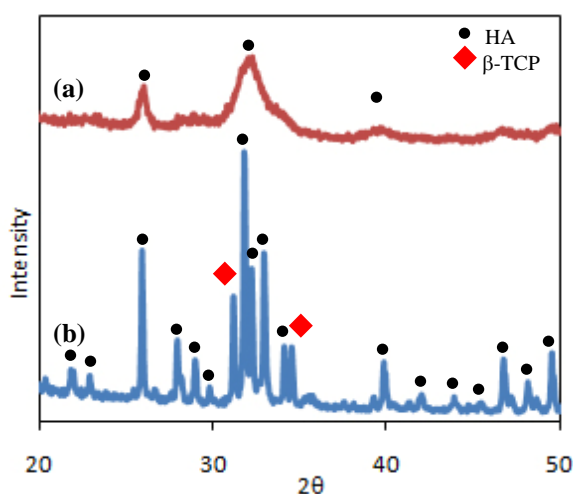


Figure 2 X-ray diffraction patterns for samples a) HA and (b) HA900

X-ray diffraction data was collected in order to assess phase purity. Figure 2(a) showing the XRD pattern for sample HA loosely matched the ICDD pattern # 09-432 of crystalline hydroxyapatite. The broadness of the peaks and low intensity indicate this is an amorphous apatitic phase. This is expected as during the synthesis no heating was applied which would have resulted in ordering of the structure. Figure 2 (b) shows the XRD pattern for sample HA900, revealing a majority of hydroxyapatite (HA) phase and some beta-tricalcium phosphate (β-TCP). This is attributed to the calcium deficiency in the as-precipitated apatitic phase (i.e. Ca:P < 1.67 due to lenient pH control) which results in decomposition into crystalline stoichiometric hydroxyapatite and β-TCP phases upon heating.^{8,17,18} The peaks appear narrow and more intense due to crystallisation and grain growth. Using the

peak for HA at 31.8° and β-TCP at 31.2° the Scherrer Equation revealed a crystallite size of ~ 48 nm for both phases. This is in agreement with the particle size measured in SEM images shown in Figure 1 suggesting that the nanoparticles are single crystals.

Raman spectroscopy was carried out to support crystallographic data. Figure 3 (a) represents the Raman spectrum for sample HA. The peak at 1043 cm⁻¹ corresponds to ν₃ asymmetric stretching of the P-O bond in phosphate groups of the apatitic phase [phase confirmed by XRD pattern in Figure 1(a)]. This peak may also be attributed to the ν₁ stretching of the C-O bond in carbonate groups in the apatitic lattice (they replace phosphate in the apatitic lattice). This suggests that the as-precipitated phase is carbonate apatite which is unsurprising as water used in reactions was not degassed prior to reactions and may contain dissolved carbonate. Indeed, carbonate substituted hydroxyapatite has been suggested as an ideal bone substitute.¹⁹ The peak at 957 cm⁻¹ corresponds to ν₁ symmetric stretching mode of the P-O bond in phosphate groups of apatite. More peaks at 577 and 420 cm⁻¹ correspond to the ν₄ and ν₂ bending modes of the O-P-O linkages in apatite, respectively. It was observed that after heat treatment at 900 °C for 1 hour [in Figure 3 (b) for sample HA900] that the peaks were better resolved. This is possibly due to higher crystallinity. The peak observed in Figure 3(a) at 1043 cm⁻¹ decreased in intensity and resolved to give to peaks at 1051 and 1026 cm⁻¹ corresponding to the ν₃ asymmetric stretching of the P-O bond in phosphate group in Figure 3(b). This decrease in intensity is probably due to loss of carbonate upon heat treatment at 900 °C for 1 hour. Another peak at 960 cm⁻¹ attributed to ν₁ symmetric stretching mode of the P-O bond in phosphate group was also observed. As Figure 2(b) shows that after heat treatment a biphasic mixture is observed, it should be noted that peaks corresponding to P-O and O-P-O vibrations can be from both hydroxyapatite and beta-tricalcium phosphate.

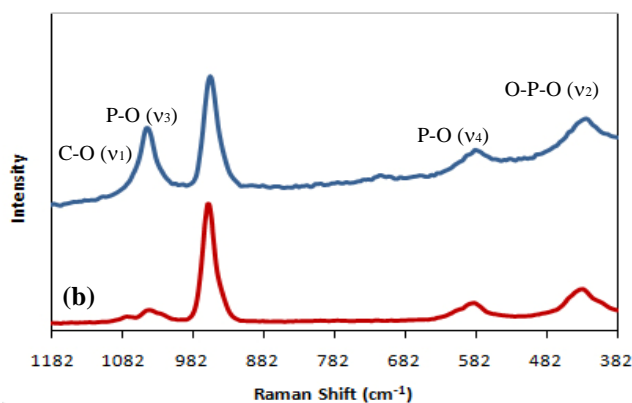


Figure 3 Raman Spectra for samples a) HA and (b) HA900

Photoacoustic Fourier Transform Infra Red Spectroscopy was carried to further assist structural characterisation. Figure 4(a) (for sample HA) reveals a wide band centred at ca. 3200 cm⁻¹ corresponding to adsorbed (or lattice) water in apatite. This band is typical of amorphous apatites synthesised using the co-precipitation technique. The peak at 1612 cm⁻¹ corresponds to ν₂ bending mode of adsorbed water. The band in the range 1530-1250 cm⁻¹ corresponds to ν₃ asymmetric stretching of the C-O

bond in carbonate in apatite. The band in the range 1200-960 cm^{-1} corresponds to ν_3 asymmetric stretching of the P-O bond in phosphate groups of apatite where as the shoulder at 959 cm^{-1} corresponds to the ν_1 symmetric stretching of the same bond. The peak at 869 cm^{-1} can be attributed to ν_2 bending mode of the O-C-O linkage in carbonate in apatite. This supplements information provided by Raman spectrum in Figure 3(a) wherein a carbonate peak was also seen. The peaks at 582, 559 and 520 cm^{-1} correspond to the bending modes of the O-P-O linkage in phosphate groups of apatite. After heat treatment it can be noticed that the large band associated with water resolves into a much finer peak at 3568 cm^{-1} as observed in Figure 3 (b) [for sample HA900]. This is due to crystallization of the amorphous apatitic phase into HA and corresponds to the (ν_s) stretching mode of the O-H group in HA. Furthermore the peaks associated to water and carbonate groups in apatite were not observed in Figure 3(c). This is understandable as heating at 900 $^\circ\text{C}$ for 1 hour will ensure loss of water and carbonate from the HA lattice. A new peak was observed at 624 cm^{-1} corresponding to the (ν_L) librational mode of the O-H group in hydroxyapatite. Appearance of this peak alongwith the peak at 3568 cm^{-1} (corresponding to O-H stretching in HA) is a subsequent of crystallization of an amorphous apatitic phase. The peaks at 597, 563 and 505 correspond to the bending modes of O-P-O linkage in phosphate group of HA. XRD data presented in Figure 2 (b) shows that a biphasic mixture of beta-TCP and hydroxyapatite was obtained after heat treatment. Therefore, it should be noted that P-O and O-P-O vibrations from these different phases may be superimposed into each other thereby not identifiable separately in FTIR spectra.

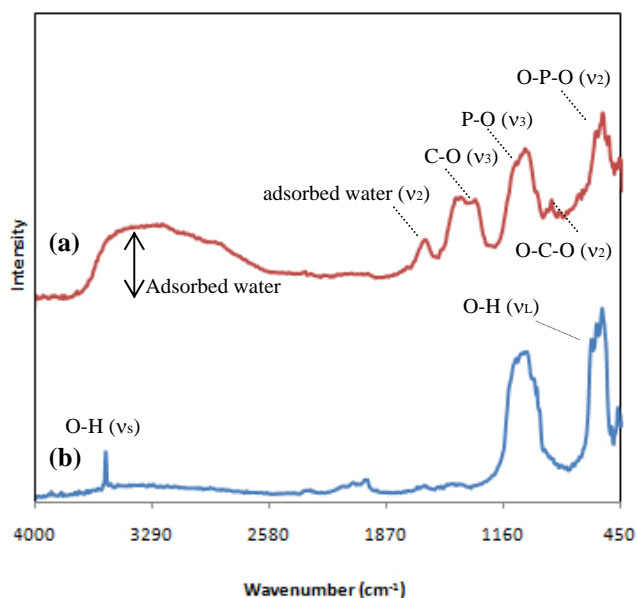


Figure 4 Fourier Transform Infra Red Spectra for sample A a) as-precipitated and (b) after heat-treatment at 900 $^\circ\text{C}$ for 1 hour.

Conclusions

This paper outlines the synthesis of amorphous non-stoichiometric HA which crystallizes into a biphasic mixture of HA and β -TCP upon heating at 900 $^\circ\text{C}$. Biphasic calcium

phosphates are desirable for applications where higher solubility of the calcium phosphates is required; β -TCP is resorbable as compared to the slow dissolving HA. SEM images reveal a rounded morphology for as-precipitated apatitic nanoparticles. Heat treatment at 900 $^\circ\text{C}$ for just 1 hour resulted in formation of nanoporous agglomerates depicting high sinterability. Raman and FTIR spectroscopy revealed the presence of carbonate ions in the apatitic phase. The first step of a calcium phosphate interface in a physiological environment is its carbonation. Therefore, the as precipitated apatitic phase has great potential for use in bone regeneration. Efforts towards *in vitro* and *in vivo* testing of such calcium phosphates developed at IRCBM, CIIT Lahore will be reported in due course.

Acknowledgements

COMSATS Institute of Information Technology is acknowledged for its research funding. Prof. Dr. S. M. Awais (SI) of KEMU/Mayo Hospital Lahore is thanked for his help regarding clinical input into the experimental design. Dr. J. A. Darr of Department of Chemistry, UCL, London, UK is thanked for his help regarding the writing of this paper.

References

- [1] A. E. Porter, S. M. Best, W. Bonfield, *J. Biomed. Mater. Res.* **2004**, 68A, 133.
- [2] F. H. Albee, *Annals of Surgery* **1920**, 71, 32.
- [3] H. Aoki, *Science and Medical Applications of Hydroxyapatite*, Japanese Association of Apatite Sciences (JAAS), Takayama Press Centre Co. **1991**.
- [4] L. L. Hench, *Journal of the American Ceramic Society* **1991**, 74, 1487.
- [5] H. R. Stanley, L. Hench, R. Goings, C. Bennett, S. J. Chellemi, C. King, N. Ingersoll, E. Ethridge, K. Kreutziger, *Oral Surgery, Oral Medicine, Oral Pathology* **1976**, 42, 339.
- [6] W. P. Cao, L. L. Hench, *Ceramics International* **1996**, 22, 493.
- [7] L. L. Hench, *Journal of the American Ceramic Society* **1998**, 81, 1705.
- [8] M. Andres-Verges, C. Fernandez-Gonzalez, M. Martinez-Gallego, *Journal of the European Ceramic Society* **1998**, 18, 1245.
- [9] A. A. Chaudhry, S. Haque, S. Kellici, P. Boldrin, I. Rehman, A. K. Fazal, J. A. Darr, *Chemical Communications* **2006**, 2286.
- [10] L. L. Hench, *Current Opinion in Solid State & Materials Science* **1997**, 2, 604.
- [11] A. A. Chaudhry, J. Goodall, M. Vickers, J. K. Cockcroft, I. Rehman, J. C. Knowles, J. A. Darr, *Journal of Materials Chemistry* **2008**, 18, 5900.
- [12] M. J. Phillips, J. A. Darr, Z. B. Luklinska, I. Rehman, *Journal of Materials Science-Materials in Medicine* **2003**, 14, 875.
- [13] A. J. Coreno, A. O. Coreno, R. J. J. Cruz, C. C. Rodriguez, *Optical Materials* **2005**, 27, 1281.
- [14] J. A. Darr, Z. X. Guo, V. Raman, M. Bououdina, I. U. Rehman, *Chemical Communications* **2004**, 696.
- [15] S. Bansal, V. Chauhan, S. Sharma, R. Maheshwari, A. Juyal, S. Raghuvanshi, *Indian Journal of Orthopedics* **2009**, 43, 234.
- [16] H. Oonishi, H. Ohashi, H. Oonishi, S. C. Kim, *Clinical Orthopaedics and Related Research* **2008**, 466, 373.
- [17] A. Siddharthan, S. K. Seshadri, T. S. S. Kumar, *Journal of Materials Science-Materials in Medicine* **2004**, 15, 1279.
- [18] A. Siddharthan, S. K. Seshadri, T. S. Samphath Kuma, Rapid Synthesis of Calcium Deficient Hydroxyapatite Nanoparticles by Microwave Irradiation, in **2005**, 110.
- [19] E. Landi, G. Celotti, G. Logroscino, A. Tampieri, *Journal of the European Ceramic Society* **2003**, 23, 2931.